Analytica Chimica Acta 749 (2012) 1–15

Contents lists available at SciVerse ScienceDirect

Analytica Chimica Acta

journal homepage: www.elsevier.com/locate/aca

Review

Silicon nanowire biosensor and its applications in disease diagnostics: A review

Guo-Jun Zhang*, Yong Ning*

School of Laboratory Medicine, Hubei University of Chinese Medicine, 1 Huangjia Lake West Road, Wuhan 430065, China

HIGHLIGHTS

- SiNW biosensor has been developed as a sensitive, label-free, electrical tool.
- SiNW biosensor has been applied to the detection of important biomarkers.
- SiNW biosensor shows a potential of miniaturization and integration.
- SiNW biosensor indicates a promising POC device for disease diagnostics.
- The diseases can include cancer, cardiovascular disease, and infectious disease.

GRAPHICAL ABSTRACT

A typical SiNW FET-based biosensor for detecting biomolecules.

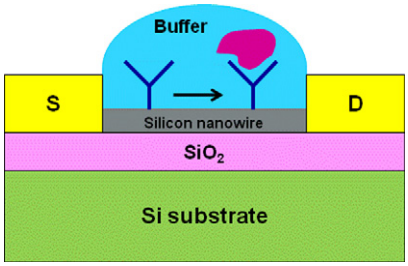

ARTICLE INFO

Article history:
Received 8 May 2012
Received in revised form 30 July 2012
Accepted 20 August 2012
Available online 28 August 2012

Keywords:
Silicon nanowire
Biosensor
Disease
Diagnostics

ABSTRACT

Over the past decade, silicon nanowire (SiNW) biosensors have been studied for the detection of biological molecules as highly sensitive, label-free, and electrical tools. Herein we present a comprehensive review about the fabrication of SiNW biosensors and their applications in disease diagnostics. We discuss the detection of important biomarkers related to diseases including cancer, cardiovascular diseases, and infectious diseases. SiNW biosensors hold great promise to realize point-of-care (POC) devices for disease diagnostics with potential for miniaturization and integration.

Contents

* Corresponding authors. Tel.: +86 27 68890259; fax: +86 27 68890071.
E-mail addresses: zhanggj@hbtcm.edu.cn, gjzhangtj@hotmail.com (G.-J. Zhang), ningyong128@163.com (Y. Ning).

0003-2670/$ – see front matter © 2012 Elsevier B.V. All rights reserved.
http://dx.doi.org/10.1016/j.aca.2012.08.035

Guo-Jun Zhang got a PhD degree in Medicine from the Tongji Medical School of Huazhong University of Science and Technology, PR China, in 1999. From 1999 to 2004, he was a Postdoctoral Fellow at Wuhan University of PR China, Institute for Physical High Technology Jena of Germany, Waseda University of Japan, respectively. Afterwards, he became a Visiting Lecturer in 2004, a Visiting Associate Professor in 2005 at Waseda University, Japan, and Member of Technical Staff in 2006 at Institute of Microelectronics, Singapore, respectively. He is currently working as a professor at Hubei University of Chinese Medicine, China.

Yong Ning got a PhD degree in Medicine from the Tongji Medical School of Huazhong University of Science and Technology, PR China, in 2004. He is currently working as a professor at Hubei University of Chinese Medicine, China.

1. Introduction

Effective disease diagnosis is essential for disease identification and subsequent adequate treatment. Currently, many diseases are diagnosed based on a variety of symptoms, which may cause late detection or be misleading, due to their subjective nature and the uncertain relationship to the disease state. Biomarkers, biological molecules including nucleic acids, proteins, peptides, or cells for example, are more closely linked to the underlying cause of disease. Disease diagnosis can be accomplished by routinely screening for important disease biomarkers. Therefore detection of the disease biomarkers is crucial, giving doctors a more objective and quantifiable basis for clinical decision-making. Point-of-care (POC) diagnostic devices present a viable method for the rapid and sensitive detection and analysis of disease-related biomarkers. Compared to classical lab instrumentation, the biosensors are being increasingly exploited as promising diagnostic devices, allowing simple, inexpensive POC testing.

Nanostructures, such as nanowires (NWs) [1,2], carbon nanotubes (NTs) [3,4] and nanoparticles [5,6], have been intensely studied for biosensing, since their diameters are comparable to the sizes of chemical and biological species to be sensed. Nanoparticles, as alternative labeling to fluorescent dyes, have been widely used for the detection of biomarkers with high sensitivity. However, this method still suffers from the requirements of target-labeling, which is time-consuming and probably causes conformational alterations or steric hindrance, induced by the additional label. One-dimensional structures such as the NWs and NTs offer opportunities for real-time and label-free sensing applications. Attractively, they are also amenable to large scale and high-density integration. SiNW-based sensors in particular, have attracted much attention due to their capabilities in sensitive detection of biological and chemical species, coupled to their manufacturability for mass production, benefiting from mature fabrication technologies [7].

SiNW sensors are typical field effect transistor (FET)-based devices, which are composed of source, drain and gate electrodes. The sensing mechanism can be understood in terms of the change in charge density, which induces a change in the electric field at the SiNW surface. For instance, biomolecules with a negative charge that bind to the surface of a n-type FET leads to an increase in the device resistance. Thanks to the large surface-to-volume ratio, tunable electrical properties, and biocompatibility, the SiNWs have been proven to be ultrasensitive and selective sensors for direct and label-free detection of metal ions [1,8], nucleic acids [9–20], proteins [1,21–30], protein–DNA interactions [31,32], small molecule–protein interactions [33], cells [34–36], and virus [37]. The performance of SiNW devices is summarized in Table 1.

Because of the important applications of the SiNW biosensor in disease diagnosis, we present herein a comprehensive review about the principle of the SiNW biosensor, the fabrication of the device, the functionalization of its surface, and the detection of disease-related biomarkers. We believe that SiNW biosensors will be used as state-of-the-art POC devices in laboratory medicine for label-free, sensitive, early diagnosis of diseases, with the potential of miniaturization and integration with fluidic and electronic circuits.

2. Silicon nanowire biosensor

2.1. Working principle

SiNW sensors are typical FET-based devices, which contain source, drain and gate electrodes. The source and drain electrodes bridge the semiconductor channel, while the gate electrode modulates the channel conductance. The SiNW connected between the source and the drain in the semiconductor channel serves as the sensing component of the device. The typical structure of SiNW

Table 1
Analytical performance of SiNW biosensors.

Device specification	Fabrication	Mechanism	Application	Detection Limit	References
p-Type SiNW; diameter: 20 nm	Bottom-up	Biotin–avidin binding	Streptavidin	10 pM	[1]
n-Type SiNW, p-type SiNW; diameter: 20 nm	Bottom-up	Antibody–antigen interaction	PSA, CEA, Mucin-1	PSA: 2 fM, CEA: 0.55 fM, Mucin-1: 0.49 fM	[21]
p-Type SiNW; diameter: 20 nm	Bottom-up	PNA–DNA hybridization	DNA	10 fM	[9]
p-Type SiNW; diameter: 20 nm	Bottom-up	Antibody–virus interaction	Influenza A virus	Single virus	[37]
n-Type SiNW, p-type SiNW; thickness: 40 nm, width: 50–150 nm	Top-down	Biotin–avidin binding	Streptavidin	10 fM	[22,55]
n-Type SiNW, p-type SiNW; thickness: 40 nm, width: 50–150 nm	Top-down	Antibody–antigen interaction	PSA, CA 15.3	PSA: 2.5 ng mL^{-1}, CA 15.3: 30 U mL^{-1}	[60]
n-Type SiNW, p-type SiNW; width: 20 nm, length: 30 nm	Top-down	DNA–DNA hybridization	DNA	10 pM	[13]
n-Type SiNW, p-type SiNW; width: 50 nm, length: 20 nm	Top-down	DNA–DNA hybridization	DNA	25 pM	[10,11]
n-Type SiNW; thickness: ≤40 nm	Top-down	Antibody–antigen interaction	PSA	30 aM	[23]
p-Type SiNW; diameter: 30–60 nm	Bottom-up	Protein–protein interaction	TnI	7 nM	[29]
n-Type SiNW; width: 50 nm, thickness: 60 nm, length: 100 nm	Top-down	PNA–DNA hybridization	DNA	10 fM	[14,16]
n-Type SiNW; width: 50 nm, thickness: 60 nm, length: 100 nm	Top-down	Antibody–antigen interaction	cTnT	1 fg mL^{-1}	[24]
n-Type SiNW; width: 50 nm, thickness: 60 nm, length: 100 nm	Top-down	PNA–DNA hybridization	RT-PCR product of DEN-2	10 fM	[19]
n-Type SiNW; width: 50 nm, thickness: 60 nm, length: 100 nm	Top-down	PNA–RNA hybridization	microRNA	1 fM	[17]
n-Type SiNW; width: 50 nm, thickness: 60 nm, length: 100 nm	Top-down	Protein–DNA interaction	ERα	10 fM	[32]
n-Type SiNW; width: 50 nm, thickness: 60 nm, length: 100 nm	Top-down	Antibody–antigen interaction	cTnT, CK-MM, CK-MB	1 pg mL^{-1}	[30]

biosensors for the detection of biomolecules is illustrated in Fig. 1a. To detect a specific target, a receptor molecule, which recognizes the target molecule, is immobilized on the SiNW surface. As shown in Fig. 1b, taking the example of a n-type immunologically modified SiNW sensor, the semiconductor channel has a uniform conductance determined by the electron density. When the surface receptors are exposed to the target molecule, carrying negative charges, specific binding will lead to a decrease in conductance. The electronic detection system then collects the conductance. This principle can be extrapolated to p-type SiNWs and positively charged biomolecules.

2.2. Fabrication of silicon nanowire biosensors

Two main nano-fabrication processes, top-down or bottom-up approaches, have been used to produce semiconducting NWs biosensor. The performance of the SiNW biosensor is influenced by many factors, such as diameters, carrier densities and mobilities, and surface chemistry. It was found experimentally that smaller diameters resulted in a greater sensitivity [11]. Similarly simulation results revealed that the minimum amount of analytes required for a detectable signal decreases when the diameter of the sensor decreases (below 10 nm in diameter) [11]. In addition, theoretical analysis indicated that the doping density determined the biosensor sensitivity [38]. For instance, lightly doped NWs show greater sensitivity than highly doped or undoped ones. These findings indicate the importance of the NW fabrication process to obtain small dimensions and appropriate doping densities in order to achieve high levels of sensitivity.

Bottom-up techniques, such as vapor–liquid–solid (VLS), have been widely reported to grow SiNWs, along with their applications as biosensors [39]. 20 nm n-type or p-type SiNWs have been produced by the VLS method, using Au nanoclusters as a catalyst and diborane or phosphine as dopant precursors. In principle, the technique allows the growth of NWs on a wide range of substrates, the most common substrates being Si wafers. High quality NWs have been produced, but their orientations on the substrate were random and their dimensions varied significantly, leading to poor device uniformity and low fabrication yield. It is a challenging task in itself to bring such techniques to manufacturing maturity. To reap the potential of SiNWs in sensor applications in a large scale, it is important to develop technologies that can reliably produce them.

To produce nanowire structures, top-down technologies use nanofabrication tools such as e-beam lithography [10,13,22,29,40–48], lithographically patterned NW electrodeposition (LPNE) [49], nano-stencil lithography [50], or nanoimprint lithography [51]. Various sizes of NWs have been produced by the e-beam lithography-based methods, with typical widths of 50 nm and lengths ranging from 20 μm to 1 mm [10,22]. Superlattice NW pattern transfer (SNAP) method had been used to create highly aligned, 20-nm-wide NWs on n- or p-doped silicon-on-insulator (SOI) wafers [13]. Penner and coworkers developed a process to prepare patterned metal nanowires using LPNE, which combines the attributes of photolithography and the versatility of bottom-up electrochemical deposition [49]. The nanowires showed a rectangular cross section and the height and width could be independently controlled as a function of trench height and electrodeposition time, down to about 20 nm in width and 6 nm in height. Engstrom et al. used aligned wafer scale nano-stencil lithography to deposit catalyst materials for the SiNW on prefabricated AFM probes. Individual vertical SiNWs were grown epitaxially by a catalytic VLS process on the AFM probes [50]. The method demonstrated a reliable and cost-efficient route towards wafer scale manufacturing of SiNW AFM probes. Vu et al. combined nanoimprint lithography with standard CMOS process to produce

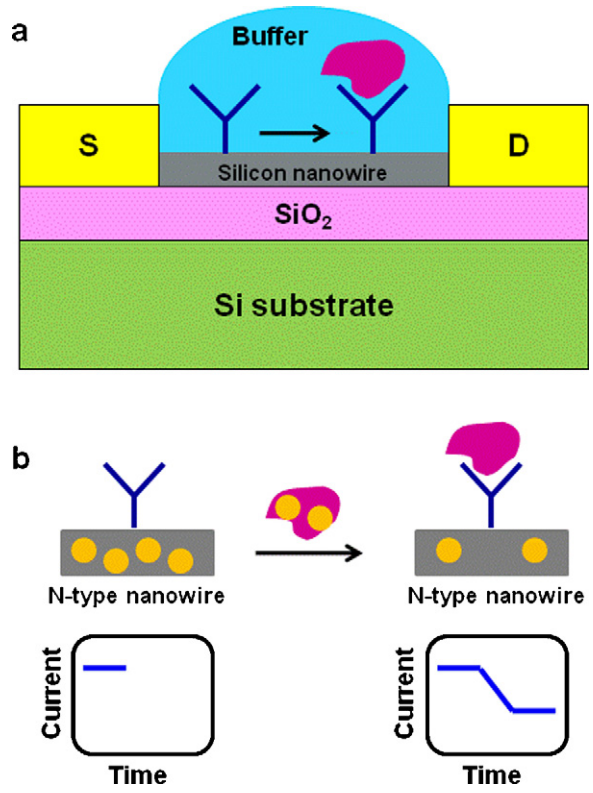

Fig. 1. Working principle of a SiNW biosensor. (a) The SiNW serving as the semiconductor channel is connected to the source and drain electrodes. The receptor molecule is immobilized on the SiNW surface and can specifically capture the target molecule. (b) When a negatively charged target molecule binds to the receptor molecule, it repels the negative charges in the region of the NW, resulting in a decrease in conductance for an n-type doped NW.

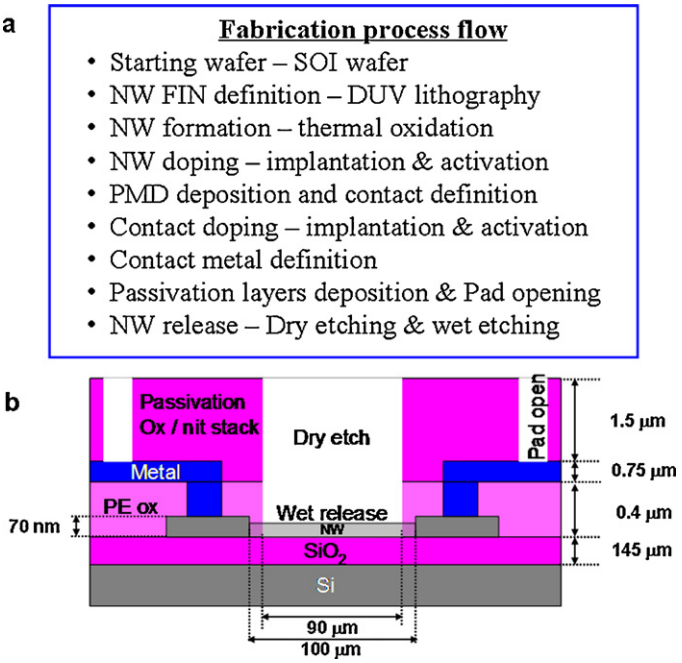

Fig. 2. (a) Schematic diagram of the fabrication process flow of a SiNW biosensor. (b) Schematic diagram of a cross-sectional view of a SiNW sensor.

large-scale SiNW arrays for biomolecular detection. The 32×32 SiNW arrays with <100 nm of SiNW diameter have been fabricated [51].

Although there is a great amount of data available on SiNW sensors, CMOS compatible SiNW devices remain challenging in terms of their manufacturability and commercialization. We have developed a top-down approach for the precise fabrication of individually addressable SiNWs in a perfectly aligned array format using CMOS compatible technology [52]. The fabrication process flow is illustrated in Fig. 2a and the cross-sectional view of a SiNW sensor is schematically illustrated in Fig. 2b. The SiNWs were formed through conventional optical lithography, etching and oxidation, which makes the process fully compatible with CMOS technology. Optical images of a wafer consisting of 72 individual SiNW sensor chips is shown in Fig. 3a, and a zoom on a single SiNW chip is provided in Fig. 3b. The chip for bio-sensing was designed as 40 clusters of 5 nanowires each. These 40 clusters were divided into 2 microfluidic chamber spaces, where the main test chamber had 36 clusters of nanowires while the control chamber had 4 clusters. Each cluster contained 5 individually addressable nanowires. The clusters were separated by a pitch of 200 μm and aluminum metal bond pads (300 μm × 300 μm, 500 μm pitch) were used for electrical connections. Scanning Electron Microscopy (SEM) micrographs (Fig. 3c) show that 5 SiNW arrays with their corresponding contact lines in one cluster are well-shaped, highly uniform and well-aligned, averaging 90 μm in length with 2 μm spacing between two wires. Transmission Electron Microscopy (TEM) images show that the width of each SiNW is appropriately 50 nm (Fig. 3d).

2.3. Surface functionalization

The surface of the SiNW has to be modified with a probe molecule so that the biosensor is capable of recognizing a specific target molecule. In order to attach the probe molecule on the surface, two approaches, electrostatic adsorption and covalent binding, have been mainly adopted for use in SiNW biosensors. In addition, Park et al. reported a novel approach to selectively functionalize the SiNW surface using joule heating, which is extremely valuable for nanowire-based sensor developments [53]. Electrostatic adsorption uses the attractive force responsible for adsorbing ionic solute on an oppositely charged adsorbent. The Heath group demonstrated DNA detection in an electrolyte solution using a SiNW sensor, in which a primary DNA strand was electrostatically adsorbed onto an amine-terminated organic monolayer on the NW surface [13].

The covalent binding method is based on the binding of the probe molecule on the SiNW surface by covalent bonds. Since oxide can grow on the SiNW surface naturally, a number of methods rely on the functionalization of the oxide layer using silane chemistry. In general, the most well-known linker molecules are alkoxysilane, of which 3-aminopropyltriethoxysilane (APTES) is the most popular one. This reagent yields amino groups on the surface that can be used to immobilize peptide nucleic acid (PNA), DNA and antibodies [17–19,24,30–32]. Likewise, the reaction of the SiNW oxidized surface with 3-mercaptopropyltrimethoxysilane (MPTMS) gives rise to a thiol (—SH)-termination. This surface can be used to immobilize DNA probes modified with acrylic phosphoramidite at the 5′ end [10]. 3-(Trimethoxysilyl)propyl aldehyde (APTMS) results in an aldehyde-terminated SiNW surface that can directly be coated with PNA, DNA and antibodies [1,9,21]. Besides alkoxysilanes, phosphonate derivatives are attractive alternative molecules to functionalize the SiNW surface with hydroxyl groups, enabling PNA to be attached [15].

In addition to using the oxide layer on the SiNW surface, this can be etched away by submerging the NWs into dilute hydrofluoric acid (HF). Stable Si—C bonds can subsequently be formed on the generated hydrogen-terminated SiNWs via

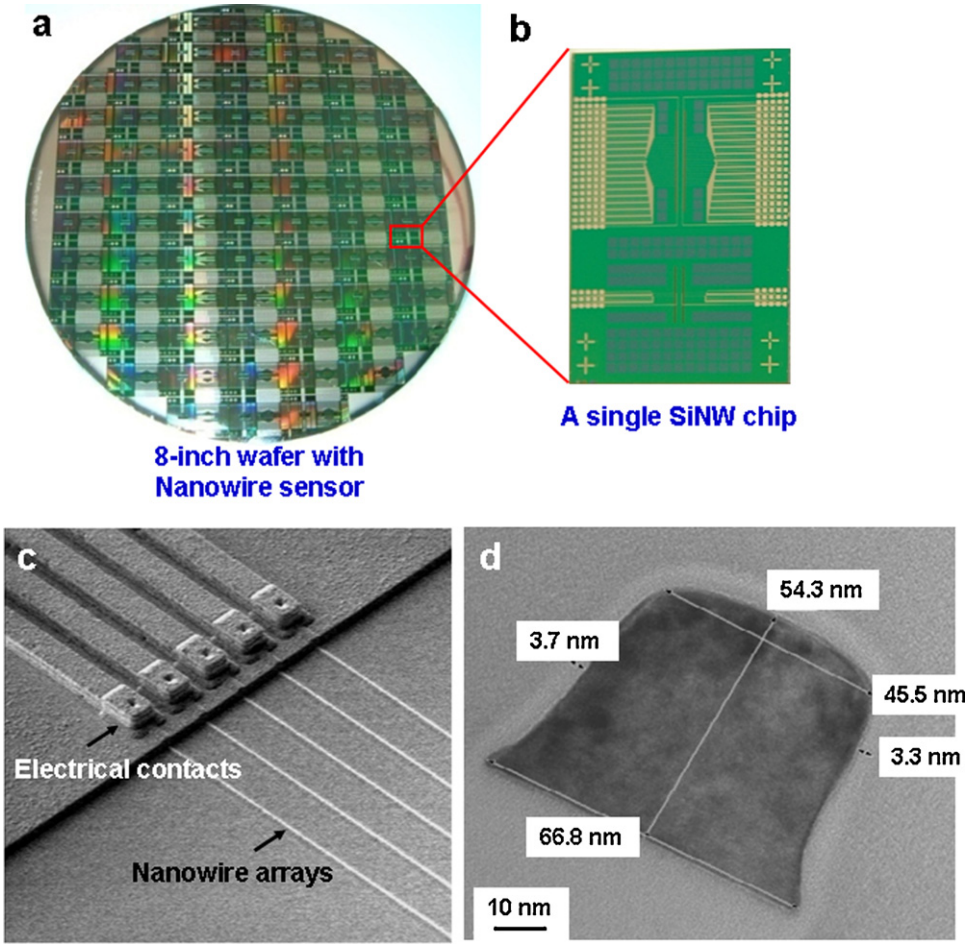

Fig. 3. (a) Optical image of an 8-in. wafer containing 72 SiNW sensor chips. (b) Zoom on a single SiNW chip. (c) SEM image of a NW cluster composed of 5 individual NWs, which are individually addressable. (d) TEM image of a single SiNW.

photochemical hydrosilylation, resulting in SiNWs coated with amino groups, which were used to immobilize probe molecules to detect proteins and DNA [8,14,16,22].

2.4. Fluid exchange

An efficient fluid exchange system is highly desirable to rapidly deliver the analyte to the SiNW surface. Two main methods for fluid exchange have been developed, using either a closed microfluidic channel or an open chamber. A polydimethylsiloxane (PDMS) microfluidic channel is commonly used and placed on the top of the SiNW sensor [2]. It directs the solution over the NW and allows a very small volume of sample to be analyzed. However, laminar microfluidic flow partially restricts the ability of the analyte molecule to reach the SiNW surface. The target biomolecule may also adsorb on the PDMS sidewalls, preventing the SiNW sensor form reaching a very high sensitivity.

We have developed a rectangular macro-scale chamber instead of a microchannel for the fluidic exchange [24]. The chamber was made out of an acrylic material and could be cut into appropriate size by using the laser machine. The assembly of the chamber on the SiNW surface was simply realized by double-sized tape. Although this method does not rely on continuous flow, the solution is delivered from a top tube to the bottom NW sensor, which avoids the slow diffusion issue, but increases detection sensitivity. In addition, a larger amount of solution can be applied. This simple design involves a reservoir which contained a volume of buffer solution sufficient to maximize binding efficiency while avoiding the diffusion limitations that microchannel systems inherently suffer from.

2.5. Debye length effect

The Debye length is an important parameter affecting the device performance. The Debye length is the distance away from the SiNW surface, over which significant charge separation can take place. Effectively, it is directly related to the distance over which the NWs can actually sense a charge. In other words, a long Debye length is desirable to ensure that less charges are screened from the NW. The Debye length can be increased by using dilute buffer solution with low electrolyte concentrations. However, excessive dilutions resulting in a low salt concentration may affect the biological activity of proteins. The Debye length, λ_D, can be calculated using the formula: $\lambda_D = 0.304(I)^{-0.5}$, where I is the ionic strength of the buffer solution used for sensing [54]. To investigate the influence of different buffer ionic strengths on detection sensitivity, a p-type SiNW biosensor was used to study biotin–streptavidin binding [55]. In this work, the effect of three increased buffer ionic strengths (decreasing λ_D) on the device sensitivity was studied for biotin–avidin recognition. When PBS diluted 1:100 in DI water ($\lambda_D \sim 7.3$ nm) was employed to bind streptavidin to surface-immobilized biotin, an increase in the device response was observed. When a 10-fold more concentrated buffer (0.1× PBS, $\lambda_D \sim 2.3$ nm) was used, the device response decreased, as streptavidin's intrinsic charge was partially screened. A further 10-fold increase in buffer ionic strength (1× PBS, $\lambda_D \sim 0.7$ nm) screened

most of the streptavidin charge, resulting in a negligible response. The results demonstrate that the electrolyte concentration in the buffer is a critical parameter to consider when optimizing the sensitivity of a FET nanosensor. We also investigated the effect of different ionic strength solution on the detection of a protein biomarker [24]. In a similar setting to the above-mentioned experiments, real time measurements on 1 fg mL^{-1} cTnT were conducted with three different buffer solutions (0.01× PBS, 0.1× PBS, 1× PBS). The addition of 1 fg mL^{-1} cTnT in 0.01× PBS resulted in a decrease in conductance, whereas the addition of 1 fg mL^{-1} cTnT in 1× PBS did not give rise to any response. A slight conductance drop was observed when 1 fg mL^{-1} cTnT in 0.1× PBS was injected. The results are in good agreement with the results on the impact of Debye screening on streptavidin sensing.

2.6. Electrical detection

To transduce the molecular binding event into a usable electrical signal, two methods have been employed: real-time detection and steady-state measurement. Both measurements were performed using an Alessi REL-6100 probe station (Cascade Microtech, Beaverton, OR) in conjunction with a HP parameter analyzer (HP-4155A). A two-probe system was set up in which a controlled voltage could be applied to the source electrode of the SiNW device while the drain electrode was referenced to ground.

For real-time detection, a short pulse voltage of 0.1 V was applied to the SiNW sensor and the current through the SiNW was measured. One data point was taken every 1 s to account for the heating effects due to power dissipation through the SiNW sensor. A buffer solution was injected into the SiNW device region through the inflow tube. The baseline was established by recording the current through the SiNW while immersed in buffer solution for 100–200 s. The biomolecule analyte solution was then added into the SiNW device region through the inflow tube, resulting in a change in conductivity due to the specific binding of the biomolecule to the functionalized surface. A stable current was achieved after 100–200 s and used to obtain the conductance of the SiNW after the binding event.

However, it is difficult to directly detect target biomolecules by the real-time method if real sample is used, because of the effect of Debye length. For instance, untreated serum usually has a short Debye length due to its high ionic strength. In this case, a steady-state measurement method is more suitable. Electrical measurements with the probe station were conducted on the SiNWs by connecting a fixed voltage source (DC-bias of 100 mV) across the source and drain electrodes of the SiNW using the same probe station as described above. The sensing experiments were carried out in an aqueous buffer solution with very low ionic strength, which was added into an acrylic reservoir attached onto the chip. The target-receptor binding was observed by recording the resistance change before and after the binding of the target molecule to the receptor molecule in the above-mentioned measuring buffer. A total of 15 wires on one chip were measured for data analysis. The sensor response was analyzed by using the formula $[(R - R_o)/R_o] \times 100$.

Besides the DC-biasing configuration mentioned above, an AC-biasing method can be used. It is one of the most popular configuration when biosensing with nanowire FETs, and consists in biasing the SiNW with AC signals and detecting the signal with the help of lock-in amplifier. Zheng et al. conducted electrical measurements using lock-in detection with a modulation frequency of 79 Hz [21], a modulation amplitude of 30 mV and a dc source-drain potential set at zero to avoid electrochemical reactions. Bunimovich et al. performed the sensing experiments using SR830 DSP Lock-in Amplifier (Stanford Research Systems Inc., Sunnyvale, CA) [13]. A 50 mV rms 13 Hz voltage source (VSD) was applied to one terminal of the nanowire, with the amplifier input operating in the current-measure mode. Wang et al. employed a detection system including a lock-in amplifier and a current pre-amplifier to record the electrical signals resulting from the binding events occurring on the SiNW-FET surface during sensing experiments [56].

3. Disease diagnostics

3.1. Cancer

3.1.1. Detection of multiple prostate cancer biomarkers

Cancer biomarkers can be used to predict the state of a tumor. The detection of specific biomarkers can be applied to cancer screening [57,58]. Since they are present in tumor tissues but only exist in the tissue or blood in extremely low concentrations, cancer biomarkers should be measured easily, reliably and cost-effectively using an assay with high analytical sensitivity and specificity. For example, one of these cancer biomarkers in wide use is prostate-specific antigen (PSA), which is produced by normal prostate cells. The higher the PSA is in serum, the higher the correlation is toward the existence of prostate cancer.

Zheng et al. reported a SiNW biosensor array that was used to detect multiple cancer biomarkers simultaneously in a single, versatile detection platform [21]. To facilitate the multiplexed detection, a larger number of individual NWs in parallel were fabricated using photolithography and metal deposition, as shown in Fig. 4a. The electrically addressable SiNW array encompassed three independent SiNW biosensors with the corresponding fluid-based assembly, on which three different antibodies were immobilized. The three antibodies were against PSA, carcinoembryonic antigen (CEA), and mucin-1, respectively, each of which is a clinically proven cancer biomarker. The real-time detection of the three cancer markers (PSA, CEA, and mucin-1) was achieved by using SiNW biosensors. The conductance-versus-time measurements showed the simultaneous recording of PSA, CEA, and mucin-1, which were delivered sequentially to the SiNW-FET arrays. As displayed in Fig. 4b, these three cancer markers induced significant signals through their binding with the cognate antibodies. By virtue of the ultrasensitive, multiplexed, real-time, and label-free SiNW-FET device, the detection limit for these three cancer markers has advanced to the pg mL^{-1} scale. Moreover, the performance of the SiNW arrays in blood serum was also investigated. As shown in Fig. 4c, the addition of serum containing PSA only resulted in a concentration-dependent conductance increase for NW 1, which was modified with an antibody specific to PSA, while serum with PSA did not lead to a conductance change for NW 2 which was passivated with ethanolamine. The simultaneous analysis of multiple biomarkers with high sensitivity could further facilitate the early detection of cancer [59], which would have a significant impact on cancer patient survival.

Kim et al. also developed an ultrasensitive and real-time method for detection of PSA using n-type SiNW FET biosensor fabricated by a top-down approach [23]. The PSA was specifically recognized by the immobilized PSA-antibody on the SiNW surface. It was found that the ultrasensitive immunodetection (below 1 fg mL^{-1}) could be achieved by controlling the dimension of the SiNW and the doping concentration of the Si channel. Very recently, Stern et al. integrated a fluidic purification chip (MPC) system and a SiNW FET array to analyze PSA as well as carbohydrate antigen 15.3 (CA 15.3) [60]. The MPC was used to pre-isolate the target molecules from whole blood by binding them to specific antibodies immobilized on the channel, subsequently cleaved by the photochemistry. The purified target molecules were then transferred to the NW cell for real-time sensing. PSA at a concentration of 2.5 ng mL^{-1} and CA 15.3 (30 U mL^{-1}) were detected from whole blood.

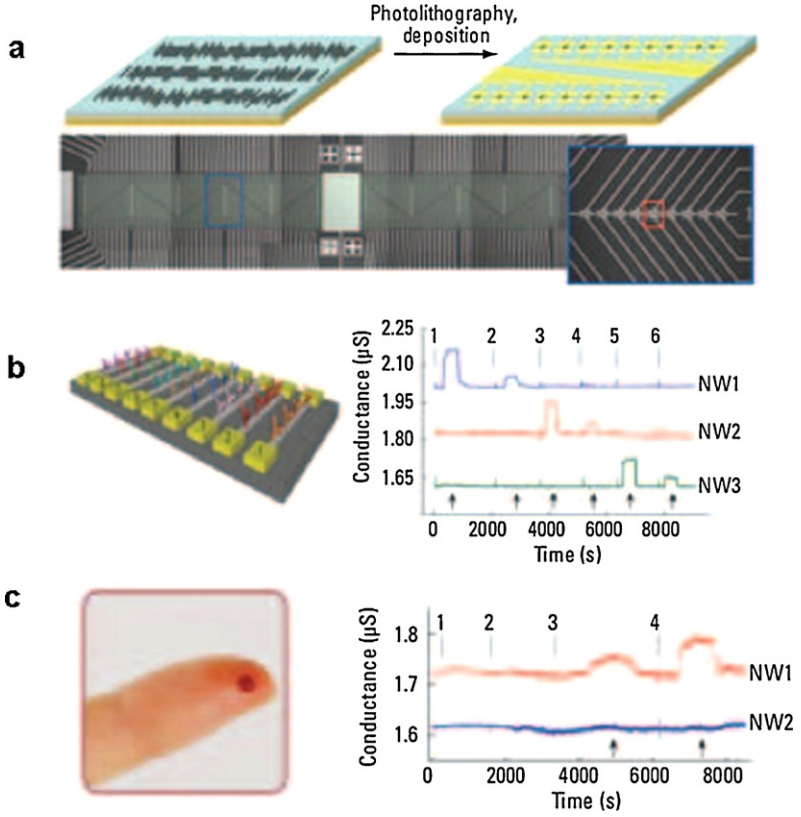

Fig. 4. (a) Optical image of a SiNW device array. (b) Schematic illustration of multiplexed protein detection by three SiNW in an array. Device 1–3 are functionalized with three different antibodies, which are specific to three different cancer biomarkers. (c) Conductance-versus-time data recorded for the simultaneous detection of PSA, CEA and mucin-1 on a SiNW array, in which NW 1–NW 3 were functionalized with antibodies for PSA, CEA and mucin-1, respectively. (d) Conductance-versus-time data recorded for the detection of PSA-containing donkey serum samples on a SiNW array, in which NW1 was functionalized with antibody for PSA and NW2 was passivated with ethanolamine. (Reprinted with permission from [7]. Copyright 2006 American Chemical Society).

3.1.2. MicroRNA detection

MicroRNAs (miRNAs), a large and growing class of 18–24-nucleotide-long non-coding RNA molecules in all known animal and plant genomes, are a key player in gene regulation. They have an important role in developmental and cell biology, including in stem cell differentiation and development [61,62]. In addition, miRNAs are clinically important biomarkers for many cancers [63]. Existing methods of detecting miRNA are dependent on hybridization with a labeled target miRNA molecule, hybridized to a complementary probe molecule. However, these methods are indirect, involving labeling of target molecules. Therefore it is critical to develop a robust method for detection of miRNAs with high sensitivity, selectivity, as well as simplicity.

We developed an ultrasensitive, direct, and label-free method for detecting microRNA [17]. Peptide nucleic acid (PNA) is neutral and does not have an anionic phosphate backbone, contrary to DNA. The repulsion between PNA and RNA is therefore less than between DNA and RNA, resulting in increased melting temperature and enhanced hybridization efficiency. As shown in Fig. 5a, PNA was covalently immobilized on the electrically addressable SiNW surface via conventional silane chemistry. After immobilization, the PNA-functionalized SiNW biosensor was used to detect miRNA. Three sequences, let-7b (complementary), let-7c (one-base mismatched), and control (non-complementary), were chosen for demonstration. The hybridization specificity of the SiNW biosensor for the detection of miRNA was demonstrated using the three sequences. It was found that the SiNW biosensor allowed for label-free discrimination between the fully matched and mismatched miRNAs, offering unique advantage over other technologies, which require labeling (Fig. 5b). Furthermore, concentration-dependent detection of let-7b by the SiNW biosensor was investigated. The SiNW resistance was recorded before and after hybridization, and the change between the two values was monitored. As shown in Fig. 5c, the more the target miRNA molecules hybridized, the higher the resistance increased. The results indicate that the biosensor is capable of detecting target miRNA at concentrations as low as 1 fM, which is one order of magnitude higher than that reported for detection of DNA [15].

The assay was further tested for the detection of miRNA in real samples by analyzing let-7b in total RNA extracted from Hela cells. The PNA-functionalized SiNW device was exposed to the total RNA aliquoted and diluted with buffer solution. Using the resistance change, the results were normalized with respect to the total RNA. The concentration of let-7b detectable in the total RNA extracted from Hela cells was $2.15 \pm 0.25 \times 10^7$ copies μg^{-1} RNA, which is in good agreement with the previously published data of miRNA expression profiling [64]. The developed detection method shows potential applications in label-free, early detection of miRNA as a biomarker in cancer diagnostics with very high sensitivity and good specificity.

3.1.3. Detection of protein–DNA interactions

The estrogen receptor α (ERα) protein is present in over two-thirds of breast cancers, where it functions in the nucleus as a ligand-dependent transcription factor to drive cell proliferation, survival, and invasiveness [65,66]. ERs mainly function as a DNA binding transcription factor that regulates gene expression. They play a key role in many normal physiological processes, but promote aberrant growth of breast cancer cells. So it is important to understand the molecular determinants regulating ER–DNA binding.

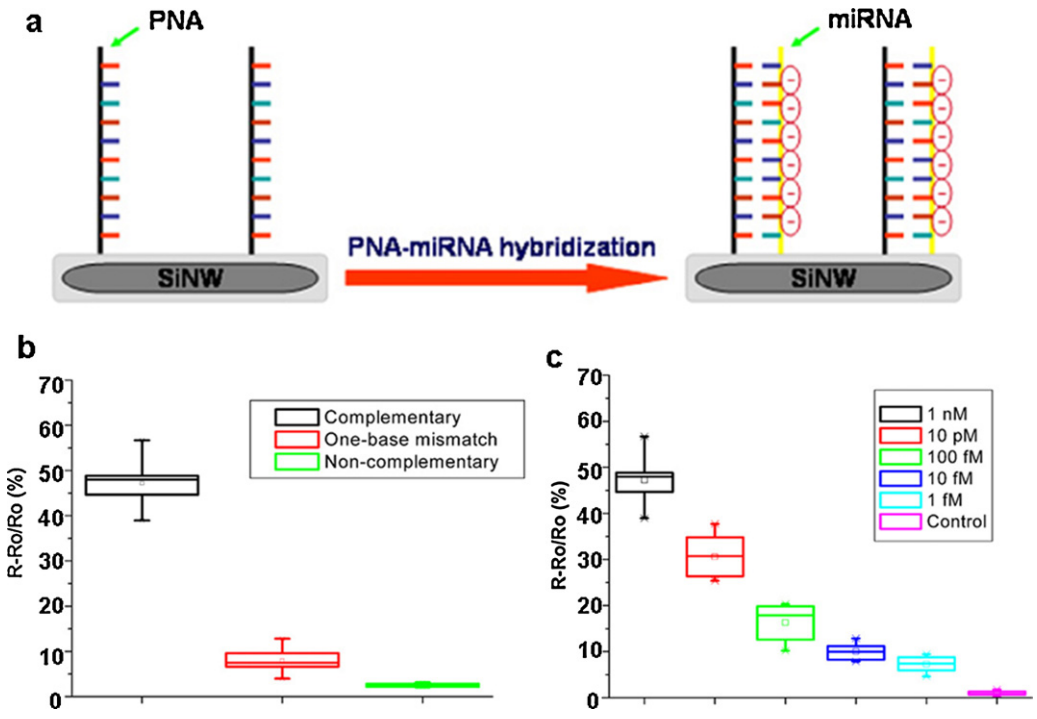

Fig. 5. (a) Schematic diagram of the PNA-functionalized SiNW biosensor for ultrasensitive detection of miRNA. (b) Hybridization specificity demonstrated by the response of the PNA-functionalized SiNW biosensors to fully complementary, one-base mismatched, and non-complementary miRNA sequences. (c) Response of the PNA-functionalized SiNW biosensors to complementary miRNA at different concentrations. (Reprinted with permission from [17]. Copyright 2009 Elsevier Science).

We developed a self-assembled monolayer (SAM)-assisted SiNW biosensor for the specific and highly sensitive detection of ER–DNA interactions, remarkably in nuclear extracts prepared from breast cancer cells [32]. As illustrated in Fig. 6a, the SiNW biosensor surface was coated with a vinyl-terminated SAM, and the termination of the surface was changed to carboxylic acid via oxidation. A double-stranded (ds)-DNA modified with an amine group was subsequently immobilized on the SiNW surface.

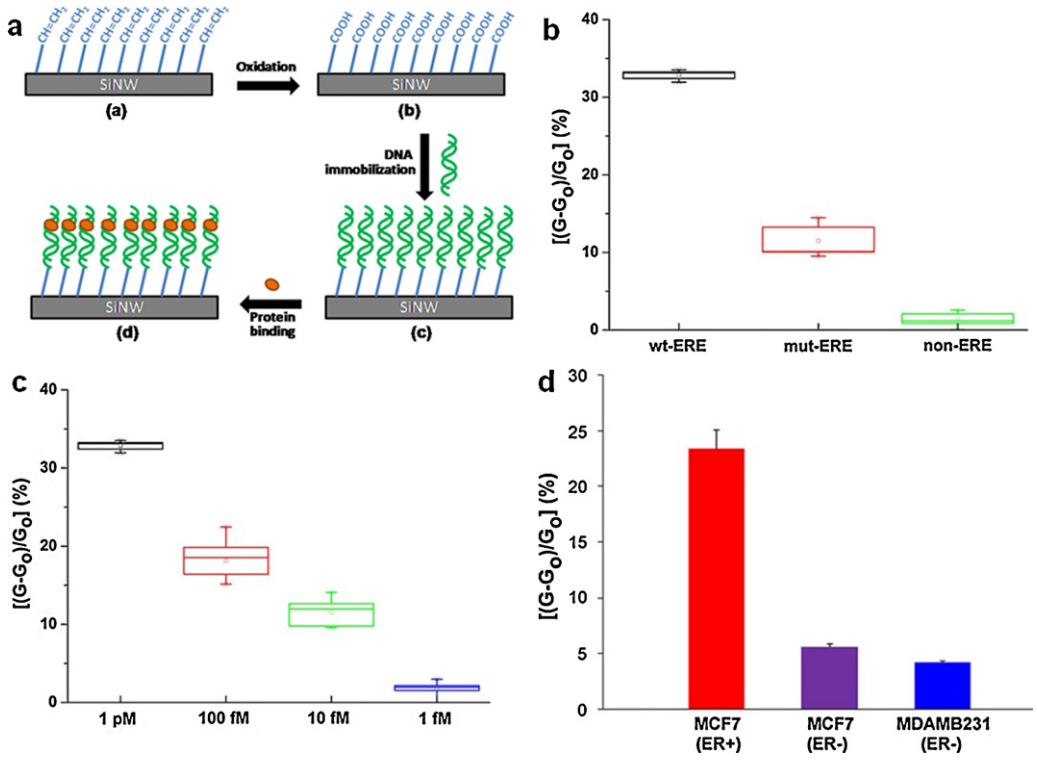

Fig. 6. (a) Schematic diagram of a SiNW biosensor for studying protein–DNA interactions. ERE is immobilized on the SiNW surface via a carboxyl-terminated SAM. ER is then bound to the specific ERE-functionalized SiNW biosensor. (b) Specificity of the interaction of ERα with three different EREs including wild-type, mutant and scrambled ERE, immobilized on the SiNW biosensor surface, respectively. (c) Response of the wt-ERE-functionalized SiNW biosensor to various concentrations of specific ERα. (d) Response of the wt-ERE-functionalized SiNW biosensor to the nuclear extracts from MCF-7 and MDA MB231 breast cancer cells. (Reprinted with permission from [32]. Copyright 2011 Elsevier Science).

We investigated the sequence-dependent binding specificity of ERα to the SiNW biosensor functionalized with three different estrogen receptor elements (EREs) including wild-type (wt), mutant and scrambled DNA sequences. The three different DNA sequences, each of which was modified with amino group at its 5′ end in the forward sequence, were immobilized on the SiNW surface via the formed SAM. As seen in Fig. 6b, a negligible change in conductance was observed when ERα was in presence of the scrambled DNA-functionalized SiNW biosensor. An obvious conductance increase was obtained upon the bonding of ERα to the wt-ERE-functionalized SiNW biosensor, while the interaction between ERα and the mutant DNA resulted in a smaller increase in conductance. We also studied the sensitivity of the detection of ERα with the wt-ERE-functionalized SiNW biosensor. Wt-ERE was immobilized on the SiNW surface and various known concentrations of ERα were used. As shown in Fig. 6c, the sensor response reduces as the solutions of ERα become more diluted. The data indicates that the wt-ERE-functionalized SiNW biosensor can achieve a limit of detection (LOD) as low as 10 fM, which is three orders of magnitude lower than that obtained by SPR-based biosensors [67].

A direct detection method for studying ER–DNA interactions in nuclear extracts from breast cancer cells was developed. Extracts from 2 breast cancer cell lines, MCF-7, that is positive for ER expression (ER+) and MDA MB231 that does not express nor shows detectable ER protein (ER−) were used. To further evaluate the specificity of the detection in the sample, ERα was knocked down by siRNA in MCF-7 breast cancer cell. Fig. 6d shows the response of the wt-ERE-functionalized SiNW biosensor to the nuclear extracts from MCF-7 and MDA MB231 breast cancer cells. As seen, a important conductance change was obtained when ERα in nuclear extracts was bound to the wt-ERE immobilized on the SiNW surface. Extracts from the knocked down cell line and the negative cell line (MDA MB 231) did not result in a significant signal. This demonstrated the capability of the SiNW biosensor for versatile applications, in particular the direct detection of protein–DNA interactions in the complex environment of real samples, which will be used to shed light on ER-mediated gene expression in breast cancer.

3.2. Cardiovascular disease

3.2.1. Troponin T detection

Cardiovascular disease (CVD) is becoming the number one cause of death globally, accounting for more than 50% of all deaths worldwide [68]. Chest pain is often thought of as a classic symptom of CVD. Patients presenting in the emergency department (ED) with chest pain usually receive an electrocardiogram (ECG) test after the patient's history has been interpreted and physical examination has been carried out. Although ECG remains the recommended test to identify patients with acute coronary syndromes (ACS), it lacks sensitivity, i.e. it cannot detect all myocardial injuries. Standard assays to detect cardiac biomarkers, such as the enzyme-linked immunosorbent assays (ELISA) are sensitive (LOD > 10 pg mL^{-1}) [69], but suffer from important sample and reagent consumption in large-scale studies. Moreover they are performed in central laboratories of clinics and hospitals and take a long time (>6 h), which is incompatible with the quick decisions needed to treat a heart attack patient. The development of new devices enabling sensitive and rapid analysis of the biomarkers could help clinicians improve their diagnostic ability as well as provide an early and accurate indication of cardiac cellular necrosis.

The cardiac troponins are more sensitive and specific than any other cardiac biomarkers for myocardial injury [70]. Human cardiac troponin-T (cTnT) is a key protein biomarker that is present in elevated concentrations in the bloodstream of a patient suffering from AMI. It is regarded, together with human cardiac troponin-I (cTnI), as the most cardiac-specific biochemical markers. CTnT is released from the cell within 3–6 h following the onset of the symptoms (chest pain). It remains elevated for 7–10 days after injury. Cardiac TnT is also an independent cardiac biomarker of cardiovascular risk in patients with ACS.

We have developed a SiNW array chip capable of detecting ultralow concentrations of cTnT in biological samples [24]. Solutions of cTnT of various concentrations were prepared by dissolving and serially diluting pure cTnT in 0.01× PBS. SiNW sensors were functionalized with anti-cTnT antibodies and individually used in experiments to detect cTnT. Fig. 7a demonstrates the real-time conductance upon injection of various concentrations of cTnT, where cTnT concentrations are decreased from 1 ng mL^{-1} to 1 fg mL^{-1}. The data was normalized by computing $G/G_{t=0}$ and plotted on the same axes for an effective comparison of the relative change in conductance. The results show that the conductance of the sensor decreases along with the concentration of cTnT. To evaluate the noise, blank buffer (0.01× PBS without cTnT) was injected into the chamber after the baseline was stabilized in the same buffer. Based on significant signal (above 3 times the background), the SiNW biosensor is able to detect as low as 1 fg mL^{-1} cTnT.

Experiments designed to test the SiNW sensor detection capabilities of cTnT in human serum were carried out to establish the potential of the system for medical point-of-care applications. A sample of raw human serum was obtained from a healthy individual with no prior history of heart disease for use in experiments to demonstrate cTnT detection in serum. The serum was desalted using a microcentrifuge filter as reported [21] and diluted back to the original protein concentration with 0.01× PBS. Various quantities of cTnT were spiked into aliquots of the desalted serum to obtain analyte solutions of the required concentrations. A graph of the SiNW conductance against time is given in Fig. 7b. Using a similar recording method as mentioned above, we observed that the conductance of the sensor immediately decreased and eventually stabilized at a lower value upon subsequent addition of the cTnT-containing serum solution. We obtained a significant change for the 300 fg mL^{-1} cTnT and an expectedly smaller change for the 30 fg mL^{-1}. It should be noted the conductance change incurred by the injection of 30 fg mL^{-1} cTnT is significant. We have thus demonstrated the label-free and real-time detection of cTnT in an undiluted serum environment down to 30 fg mL^{-1}, which is 3 orders of magnitude lower than that achieved by ELISA methods [69].

3.2.2. Multiple cardiac biomarkers detection in serum

Simultaneous assessment of multiple biomarkers would provide complementary information and enable doctors to stratify risk among patients with ACS more effectively and rapidly [71]. In these patients, cTnT, creatine kinase-MM (CK-MM) and creatine kinase-MB (CK-MB) each predict different cardiac events. Initially, discussions of cardiac biomarkers were only limited to CK-MB, aspartate aminotransferase, and lactate dehydrogenase. These enzymes are released in upon myonecrosis and thus were used as tools for the diagnosis of MI. Recently however, several new cardiac biomarkers have been studied. For example, cTnT is a more sensitive and specific marker of myocyte necrosis than CK-MB. Although each of these markers appear to reflect a unique axis in the pathobiology of ACS, little is known about the utility of these biomarkers in combination. By using POC devices, a multiple marker approach would enable doctors to rapidly stratify patients for adverse cardiac outcomes.

As discussed earlier, a low ionic strength buffer enables to extend the Debye length, preventing the screening of the electrical signals in the SiNW biosensor. To analyze cTnT in serum in real time, the serum was desalted. This additional step made real-time detection difficult to carry out. To eliminate the desalting

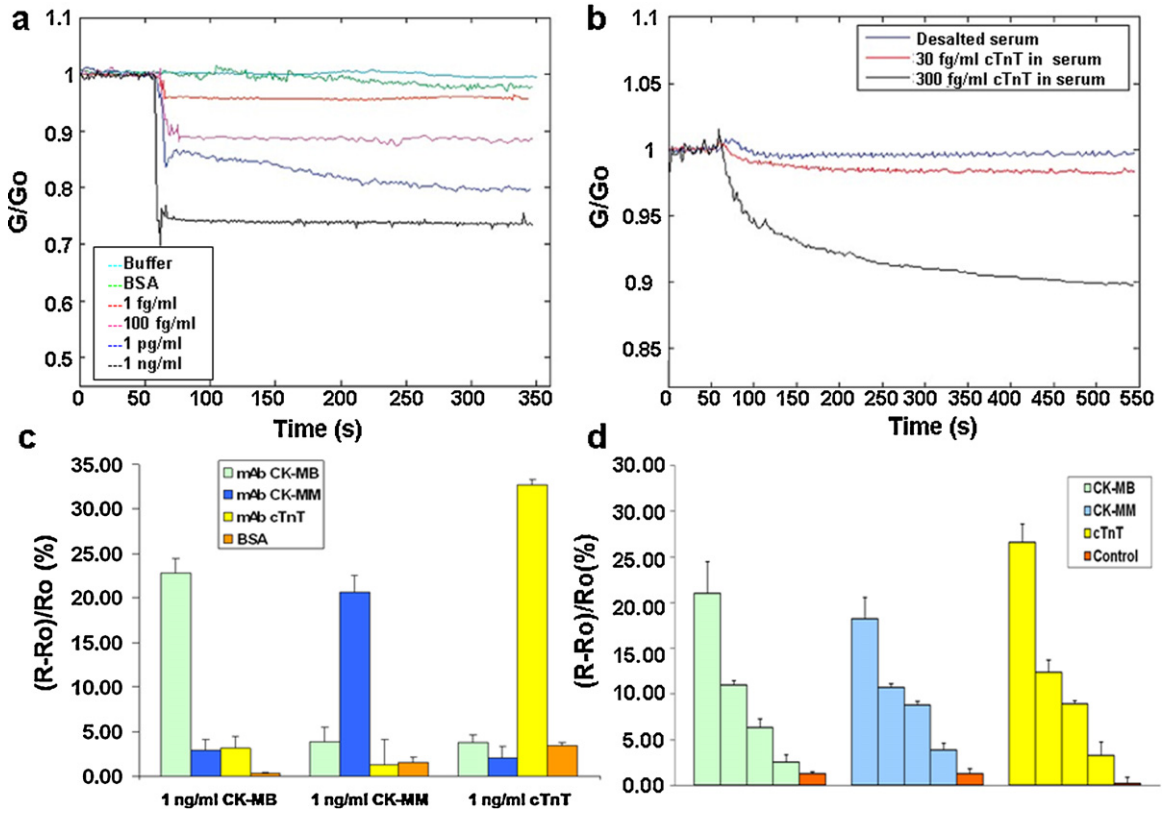

Fig. 7. (a) Real-time conductance of a SiNW sensor functionalized with anti-cTnT and used in experiments to detect cTnT in buffer. (b) Real-time conductance of a SiNW sensor functionalized with anti-cTnT and used in experiments to detect cTnT in desalted human serum. (c) Specificity of a SiNW sensor in a multiplexing format. Three biomarkers (cTnT, CK-MM and CK-MB) are sequentially incubated on the SiNW sensor spotted with the three antibodies and BSA. (d) Sensitivity of a SiNW sensor in a multiplexing format. Resistance change at different concentrations of the three biomarkers (cTnT, CK-MM and CK-MB) spiked in serum. (a and b reprinted with permission from [24]. Copyright 2009 American Chemical Society) and (c and d reprinted with permission from [72]. Copyright 2012 Elsevier Science).

process, we developed a new steady-state detection method based on the SiNW array biosensor, independent of the ionic strength of the sample solution, allowing the SiNW sensor to directly analyze the cTnT, CK-MM and CK-MB in blood serum [72]. The serum was directly incubated with the SiNW biosensor functionalized with various antibodies. To enable antibody–antigen interactions, the reaction was conducted in an untreated serum, which has high ionic strength. However, the measurement was carried out in the presence of 0.01× PBS before and after binding and the sensor response was calculated as the change in resistance after the cardiac biomarkers bound to the antibodies and the serum was replaced with low ionic strength buffer, with respect to the measurement before the serum was introduced. The cardiac biomarkers are negatively charged in a neutral PBS buffer (pH 7.4) with pIs of ~5, ~5.8 and ~6.5 for cTnT, CK-MB and CK-MM, respectively, their binding to the SiNW surface thus increased the resistance.

The SiNW biosensor comprising of NWs in an array configuration was produced as described previously. Three different antibodies against the specific cardiac biomarker, monoclonal antibody CK-MM (mAb CK-MM), monoclonal antibody CK-MB (mAb CK-MB) and monoclonal antibody troponin T (mAb cTnT), were separately spotted on the SiNW chip array to allow selective multiplexed detection. As a control, BSA was also spotted in a separate area. The binding of cardiac biomarkers to the surface-immobilized antibodies only occurred on the SiNW clusters with matching antibodies. As can be seen from Fig. 7c, when 1 ng mL^{-1} of cTnT, CK-MM and CK-MB in serum were separately incubated with the antibodies-functionalized SiNW, obvious resistance change was obtained for each corresponding specific antibody, whereas negligible change was seen in the case of non-specific antibodies. Negligible response was observed from the BSA-spotted SiNW clusters.

Serum samples spiked with the three proteins at concentrations ranging from 1 ng mL^{-1} to 10 fg mL^{-1} were incubated with the three antibodies-spotted SiNW sensors. Fig. 7d shows the sensing response with respect to concentration. An important resistance change was observed when serum spiked with 1 ng mL^{-1} of cTnT, CK-MM and CK-MB was applied, while the signal was reduced but was still detectable for 100 fg mL^{-1} of the proteins. A control serum without any protein exhibited negligible resistance change. These results demonstrate that the antibodies-functionalized SiNW sensor is capable of multiplexed detection of proteins in undiluted and untreated blood serum with high sensitivity and selectivity down to fg mL^{-1} concentrations.

3.2.3. *Integrated microsystem for protein analysis from blood*

Blood is the most important body fluid, and direct analysis of protein biomarkers from blood is playing an important role in disease diagnosis. However, not only are conventional approaches to analyzing clinical blood proteins time consuming, but they also require multiple steps and large amounts of blood. As a result, there is a demand for developing assays for sensitive, specific, multiplexed detection of protein biomarkers in blood.

We developed an integrated chip allowing rapid, sensitive, and simultaneous analysis of three cardiac biomarkers from finger-pricked blood [30]. The integrated chip is composed of a filtration chip for plasma separation from blood and a SiNW array sensor chip for protein detection. These two chips are fabricated separately and assembled into one device via back-to-back integration. The integrated chip has the advantage of reducing dead volumes by eliminating tubing connections between the two chips. After the plasma was filtered by the separation chip, the SiNW sensors,

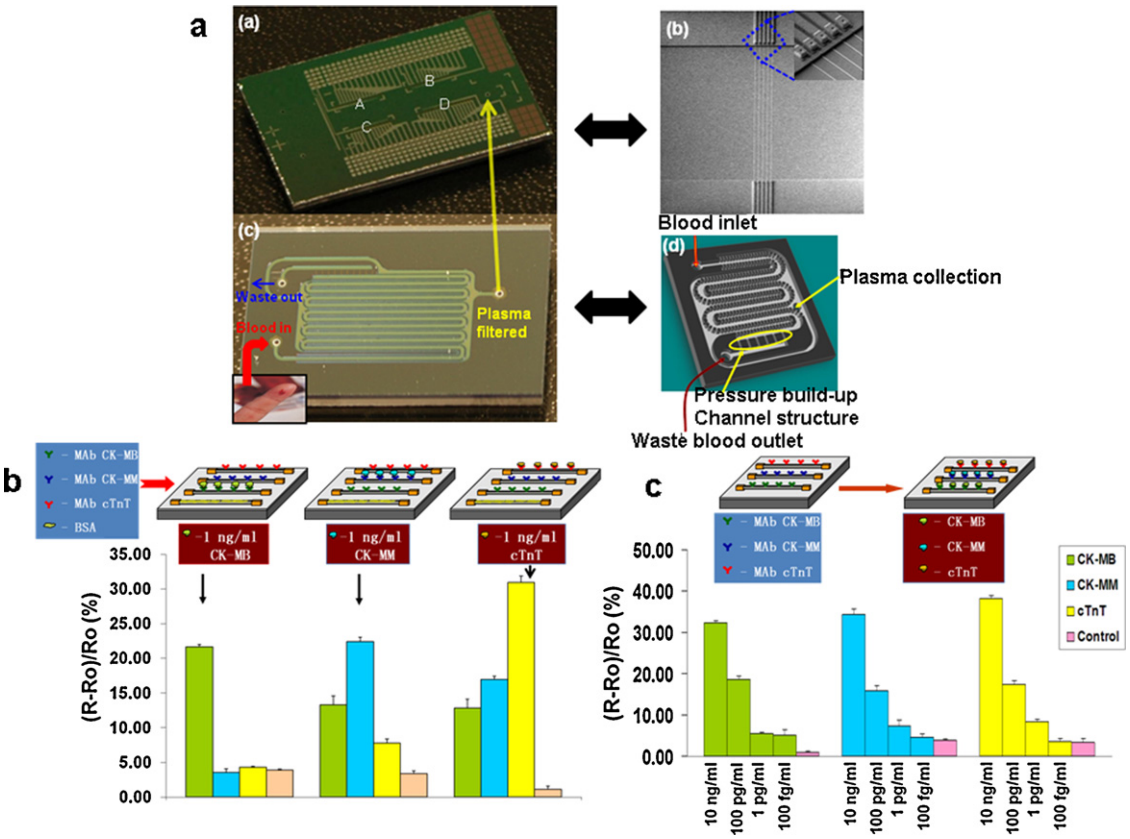

Fig. 8. [a] Design of the integrated chip. (a) Optical image of a SiNW array sensor chip. (b) SEM of a SiNW cluster consisting of five individual nanowires. Zoom on the five nanowires and their electrode connections (inset). (c) Optical photograph of a filtration chip for plasma separation from blood. (d) Schematic showing the working principle of plasma filtration from blood using the filtration chip. [b] Specificity of the integrated chip showing that individual biomarker could be distinguished from the others in blood. [c] Response of the integrated chip to various concentrations of three cardiac biomarkers spiked in blood. (Reprinted with permission from [30]. Copyright 2011 Elsevier Science).

spotted with three different antibodies, enabled us to detect three cardiac biomarkers, cTnT, CK-MM and CK-MB, simultaneously.

In order to increase the number of NW array sensors for detection to cope with the requirements of multiplexing, a new chip layout with 255 nanowires in 51 different clusters divided into 4 groups, A–D, was designed (Fig. 8a(a)). Groups A–C, each had 12 clusters (5 nanowires in one cluster) separated by a distance of 300 μm. Group D had 15 nanowire clusters with the same pitch. Each cluster was linked to 5 NW. A SEM shows the nanowires (90 μm long with a pitch of 2 μm) with their respective electrical connections (Fig. 8a(b)).

The filtration chip on the bottom side of the integrated chip was able to extract the plasma from the whole blood sample. An optical image of the filtration chip is shown in Fig. 8a(c) while a conceptual drawing of the continuous flow pillar gap structured plasma separator is shown in Fig. 8a(d). The working principle is based on the size exclusion of the cells through crossflow filtration. Only plasma was allowed to pass through the submicron gaps between the vertical pillars, which are located tangentially to the main flow path of the blood sample. Several narrow channels (10 μm in width, 300 μm in length) were introduced downstream of the main blood flow channel to build up sufficient pressure and thereby enhance the separation speed. To collect 10 μL of plasma from whole blood at an efficiency of 95% within 15 min, the input blood flow rate was set at 10–15 $\mu L\,min^{-1}$.

The three different cardiac biomarker antibodies, MAb CK-MM, MAb CK-MB, MAb cTnT were spotted separately on the chip array. As a control, BSA was also spotted on different NW. 2 μL of blood in 198 μL of 1× PBS buffer spiked with three proteins were flowed through the filtration chip. The specificity of the integrated chip was established by spiking individual cardiac biomarker (cTnT, CK-MM and CK-MB) in blood, in sequence. For instance, when cTnT was spiked in blood, only the anti-cTnT-functionalized SiNW biosensor showed a significant response, whereas the anti-CK-MM, anti-CK-MB and BSA-functionalized sensors did not give rise to any resistance change. Results in Fig. 8b show that a distinguishable resistance change was obtained for each corresponding specific antibody when 1 $ng\,mL^{-1}$ of cTnT, CK-MM and CK-MB was applied, while no change was noted for BSA. The results indicate that the integrated chip allows the proteins to be detected specifically.

The sensitivity of the integrated chip was demonstrated by spiking the three proteins at various concentrations to blood. CK-MB, CK-MM and cTnT were spiked at various concentrations into blood diluted 100 times with 1× PBS, while unspiked blood was used as a negative control Fig. 8c shows a clear trend of resistance decrease with a decrease in protein concentrations, while negligible resistance change was obtained for unspiked whole blood, indicating that the impurities in blood did not affect the detection. The results show that 1 $pg\,mL^{-1}$ could be detected, which is 1 order of magnitude lower than the conventional ELISA technique [69], and 2 orders of magnitude lower than commercially available test kits. The integrated chip enabled to achieve this low detection limit for all three biomarkers, from finger-prick blood within 45 min.

3.3. Infectious diseases

3.3.1. Dengue virus detection

Dengue is a commonly prevalent arthropod-borne viral infection throughout the world. It has four serotypes inducing a wide spectrum of non-specific symptoms that lead to Dengue Fever

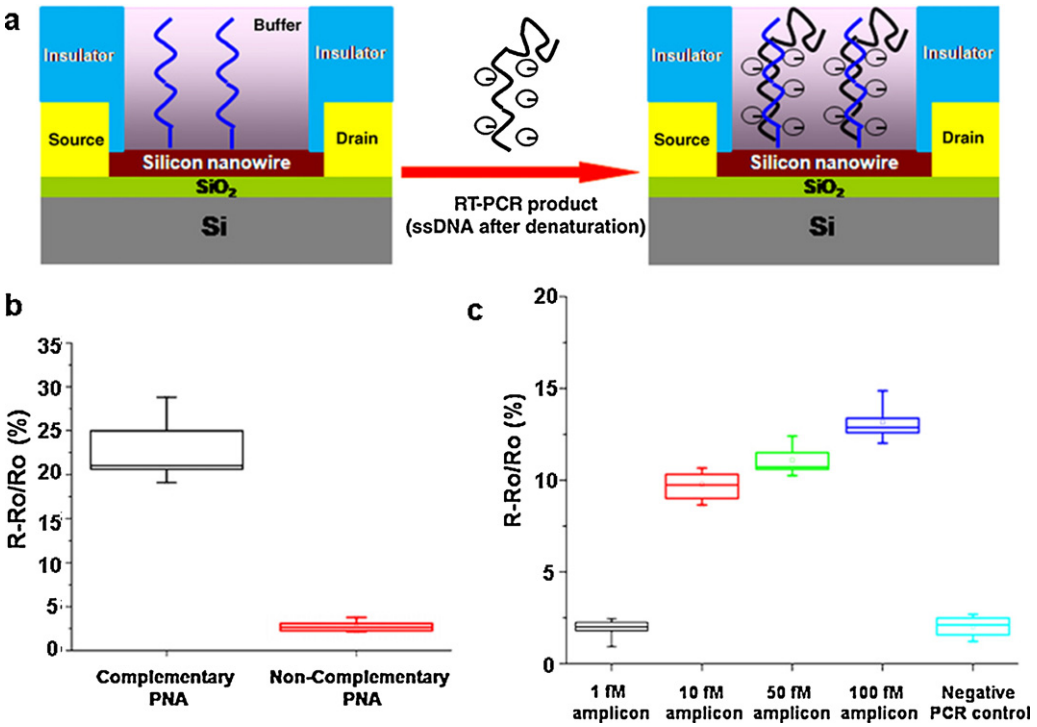

Fig. 9. (a) Schematic diagram of the RT-PCR product of DEN-2 hybridized to the PNA-functionalized SiNW biosensor. (b) Specificity of the RT-PCR product of DEN-2 to the SiNW biosensor, which is coated with the complementary and the non-complementary PNA sequences, respectively. (c) Resistance change data plotted for different concentrations of the RT-PCR product of DEN-2 using PNA-functionalized SiNW sensors. (Reprinted with permission from [19]. Copyright 2010 Elsevier Science).

(DF). Infection with any of the four serotypes of Dengue virus may cause DF [73]. No effective vaccine or specific therapeutic treatment, to date, is available for preventing or curing the disease. The two currently available methods for diagnosis, serological detection [74] and virological detection [75], are time-consuming and do not yield confirmed results early enough. Miniaturized diagnostic devices which are inexpensive and field-ready with high sensitivity and specificity are urgently needed to diagnose large populations suffering from infectious diseases and curb the spreading of the infections into pandemics.

Studies in Southeast (SE) Asia suggest that a secondary infection with dengue serotype 2 (DEN-2) virus is more likely to cause severe disease than with other serotypes [76]. We developed a novel SiNW biosensor based on PNA–DNA hybridization for highly sensitive and rapid detection of Dengue virus. Dengue virus contains a single-stranded RNA (ssRNA), which can be amplified and detected through RT-PCR. RT-PCR enables the identification of different serotypes by serotype-specific primers. The basic principle of this method is illustrated in Fig. 9a. The SiNW were functionalized with a 16-nt PNA using a previously reported surface chemistry. As a proof-of-concept, a fragment of DEN-2 (69 bp) identified in the capsid (C) region was selected and amplified by RT-PCR as the target, in which 69 bp of the RT-PCR product at the 3′ end were complementary to the immobilized PNA sequence. The RT-PCR product was double stranded DNA (dsDNA), and carried a negative charge from the phosphates ions in its backbone. The dsDNA had to be denatured to ssDNA prior to hybridization. After hybridization, the RT-PCR product of DEN-2 was bound to the PNA-functionalized SiNW, bringing about negative charges to the sensor surface. With the introduction of these negative charges, a depletion zone in the n-type FET appeared, increasing the resistance. The response before and after hybridization corresponded to the amount of RT-PCR product hybridized on the SiNW surface. This unique method can be used to detect Dengue virus in a sensitive and serotype-specific manner.

The specificity of the PNA–DNA hybridization for the detection of the RT-PCR product of DEN-2 is important with respect to the impurities of the RT-PCR product solution, which contained the primers, the sample, dNTP as well as the targeted amplicons. Two different PNA sequences, one complementary and the other one non-complementary to the RT-PCR product of DEN-2, were immobilized on the SiNW surface. As shown in Fig. 9b, an obvious increase in resistance was observed when 1 nM of the amplicons were applied to the complementary PNA-functionalized SiNW, whereas a negligible change was obtained as the same amplicons were hybridized to the non-complementary PNA-functionalized SiNW. The results reveal that the 69 bp sequence obtained by RT-PCR was specific to the complementary PNA sequence, and the hybridization occurred on the SiNW surface as anticipated.

The detection sensitivity using the SiNW biosensor was analyzed by directly applying the un-purified RT-PCR product to the PNA-functionalized SiNW sensor. Fig. 9c shows the dependence of the hybridization signals on the concentrations of the un-purified RT-PCR product of DEN-2. Since the sensor response depends on the change in surface charge after hybridization, and more charges present are associated with the increase of concentrations of the targeted amplicons. The results demonstrate that 10 fM of the amplicons in un-purified RT-PCR product can effectively and selectively be detected by the SiNW sensor within 30 min, indicating as well that the impurities in the product do not inhibit the detection. The approach shows potential for eliminating the demand for laborious methods by integrating the SiNW sensor with RT-PCR based on a silicon technology platform.

3.3.2. *Seasonal virus detection*

H1N1 2009, also named swine-originated influenza A, was a worldwide epidemic that spread from Mexico within a short time [77]. Real-time RT-PCR is the “gold standard” method for identifying the H1N1 virus. However, it requires skilled personnel in a central laboratory. Testing kits such as Binax Now, BD Directigen

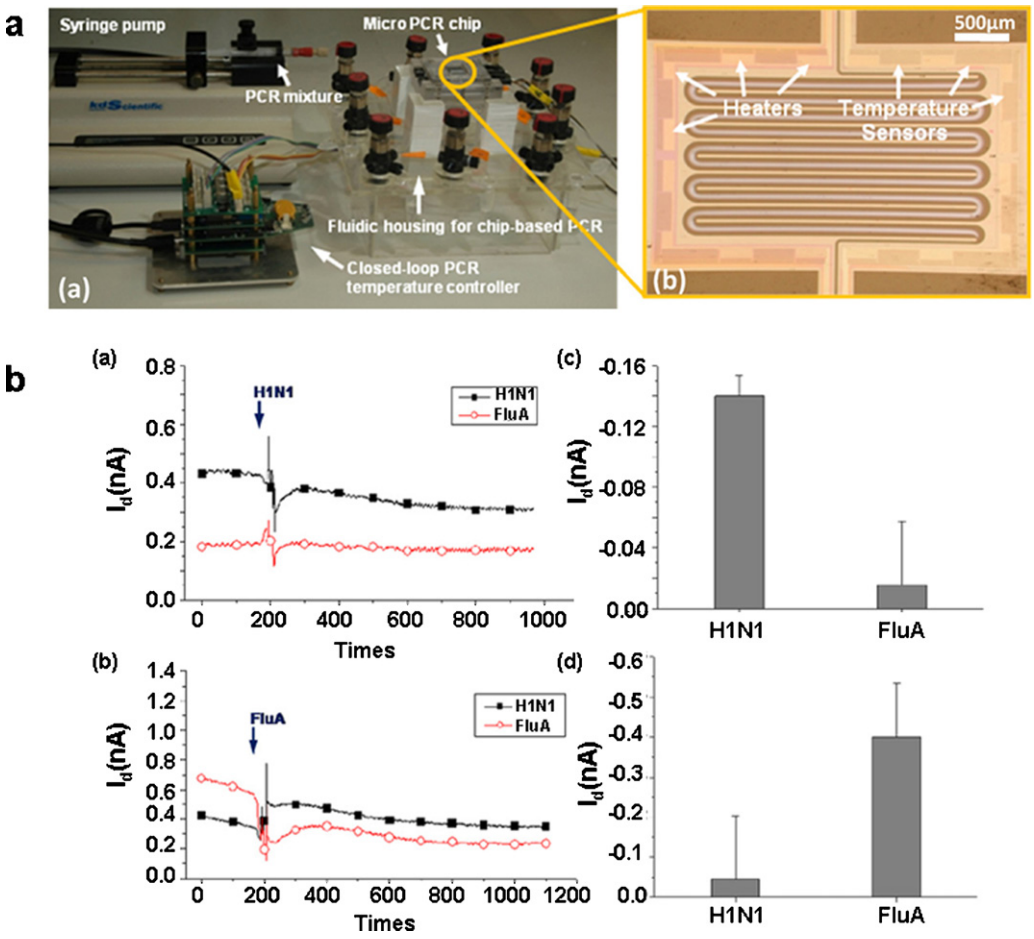

Fig. 10. [a] Setup of a microchip-based PCR. (a) A PCR chip is mounted in a fluidic housing and the sample mixture is injected into the PCR chamber via a syringe pump. The temperature cycling was controlled by a closed-loop circuit connected to a PC for user interface and data readout. (b) Optical image of the PCP chip. The micro chip chamber consists of a meander-shaped micro PCR chamber, 10 μL in volume, fluidic inlet/outlet, 4 pairs of microheaters and temperature sensors, which are located in all four corners of the micro PCR chip chamber. [b] Results of differential measurement of a SiNW biosensor. (a) and (b) Real-time conductance-versus-time for differential detection of H1N1 and FluA. (c) and (d) The average conductance change of the target SiNW sensor is about 10 times higher than the unmatched SiNW sensor. (Reprinted with permission from [79]. Copyright 2011 Elsevier Science).

EZ and Quidel QuickVue, are commercially available for screening seasonal influenza A (FluA) infection. Nevertheless, these assays suffer from low sensitivity and are not capable of distinguishing the subtypes of seasonal influenza A, e.g. seasonal influenza A (H3N2) versus novel H1N1 2009 virus [78]. Hence diagnostic tools capable of rapid and accurate identification of the H1N1 virus would have a great impact on restraining the disease right at an early stage of the outbreak and thus prevent a worldwide transmission.

Kao et al. have developed a microsystem based on SiNW biosensors and a multiplexed PCR module to differentiate subtypes of the H1N1 2009 strain versus the seasonal influenza (FluA) strain [79]. The two-module microsystem consists of multiplexed PCR to amplify nucleic acids and SiNW detection to check the sequences. As the concentration of the influenza viral RNA from the virus is very low, beyond the detection limit of the SiNW biosensor, enrichment of sufficient sample for detection is needed. The chip-based PCR module delivered 10^4–10^5 multiplexed amplification for both FluA and H1N1. The setup of the microchip-based PCR is illustrated in Fig. 10a. The microsystem was composed of the microfluidics, temperature control and a data acquisition module. The microfluidic PCR system was integrated with heaters and temperature sensors on a silicon chip to shorten the cycling time. The amplified dsDNA had to be denatured to single-stranded DNA (ssDNA) before being delivered to the SiNW biosensor for detection via molecular hybridization.

Real-time detection was employed to monitor H1N1 and FluA. To minimize the interference from the background, a reference SiNW was used as the baseline. As discussed earlier, PNA was immobilized on the SiNW biosensor surface as the probe, the PCR product containing either FluA or H1N1 amplicons were denatured and injected onto the sensor surface for detection. The real-time response of the PNA-functionalized SiNW biosensor to either H1N1 or FluA was recorded once the sample had been flowed through the microfluidic channel, as shown in Fig. 10b. The detection module demonstrated a 10 times change in the magnitude of the differential current when the target amplicon was injected. It was found that the microsystem was able to achieve a sensitivity of 20–30 fg μL^{-1} for H1N1 and FluA in a 10 μL sample. This microsystem enabled low sample consumption, high sensitivity and high specificity, which will help doctors reach a yes/no decision for infectious disease.

Patolsky et al. demonstrated the direct and real-time detection of a single virus using antibody-functionalized SiNW biosensors [37]. When the p-type SiNW biosensor immobilized with antibody for influenza A was exposed to highly dilute influenza A virus solutions, of the order of 80 attomolar or 50 viruses mL^{-1}, measurements showed discrete conductance changes, characteristic of binding and unbinding of influenza A. Moreover, the multiplexed detection of different viruses using different antibodies-modified SiNW biosensor arrays was carried out, in which influenza A and adenovirus could be detected in parallel. The work revealed the

potential for simultaneous detection of multiple viruses at the single virus level.

4. Outlook

The advantages of SiNW arrays are (i) high uniformity and reproducibility, (ii) high yield, and (iii) excellent scalability and manufacturability. In addition, fabricating the SiNW arrays by the proposed top-down approach, using standard semiconductor processing technology, makes it possible to fabricate SiNWs for both low- and high-multiplexing capabilities and permits direct integration with electrical readout circuits. Current efforts in our laboratory are dedicated to the realization of such a platform, where an electrical biosensor detection module consisting of a SiNW sensor array chip, a miniaturized electrical probe station into which the bio-chip can be slotted onto electronic circuitry which measures the resistance of the nanowire, and is interfaced with a read-out and data management system. This detection module will be of great scientific value and may offer an integrated and portable system to enable gene profiling and molecular diagnostics. In addition, as with other nanowire biosensing devices, the analytical signal intensity is still relatively low and is superimposed on a high background. The ability to increase significantly the signal intensity is important for the realization of practical SiNW sensors. Various surface chemistries are being developed in our lab to make the SiNW sensors sensitive and robust. Nonetheless, the eventual acceptance of semiconductor nanowire-based detection schemes for diagnostic applications will depend on how these novel schemes compare with the current gold standards, i.e. PCR and ELISA, in terms of simplicity, sensitivity, specificity, and reliability.

Acknowledgments

The authors would like to thank Dr. Julien Reboud (University of Glasgow, Scotland, UK) for his useful help in editing the English. The authors would also like to thank Dr. Ajay Agarwal, Dr. Eu-Jin Andy Lim, Ms. She Mein Wong, Mr. Guang Kai Ignatius Tay, and Mr. Jason Jun'An Ang of Institute of Microelectronics, Singapore, for SiNW biosensor chip fabrication; Mr. Huiyi Chua Jay, Ms. Ru-Ern Chee, Mr. Henry Zhan Hong Luo, and Ms. Joon Min Huang of Institute of Microelectronics, Singapore, for biotesting. The authors also acknowledge financial support from the Singapore Economic Development Board (COY-15-POC/1457-3) and from the Agency for Science, Technology and Research (A*STAR), Singapore (CCOG01-005-2008).

References

[1] Y. Cui, Q.Q. Wei, H.K. Park, C.M. Lieber, Science 293 (2001) 1289–1292.
[2] F. Patolsky, G. Zheng, C.M. Lieber, Nat. Protocols 1 (2006) 1711–1724.
[3] S.J. Tans, M.H. Devoret, H.J. Dai, A. Thess, R.E. Smalley, L.J. Geerligs, C. Dekker, Nature 386 (1997) 474–477.
[4] J. Kong, N.R. Franklin, C. Zhou, M.G. Chapline, S. Peng, K. Cho, H. Dai, Science 287 (2000) 622–625.
[5] A.P. Alivisatos, Science 271 (1996) 933–937.
[6] S.-J. Park, T.A. Taton, C.A. Mirkin, Science 295 (2002) 1503–1506.
[7] F. Patolsky, G. Zheng, C.M. Lieber, Anal. Chem. 78 (2006) 4260–4269.
[8] G.-J. Zhang, A. Agarwal, K.D. Buddharaju, N. Singh, Z.-Q. Gao, Appl. Phys. Lett. 90 (2007) 233903.
[9] J.-I. Hahm, C.M. Lieber, Nano Lett. 4 (2004) 51–54.
[10] Z. Li, Y. Chen, X. Li, T.I. Kamins, K. Nauka, R.S. Williams, Nano Lett. 4 (2004) 245–247.
[11] Z. Li, B. Rajendran, T.I. Kamins, X. Li, Y. Chen, R.S. Williams, Appl. Phys. A 80 (2005) 1257–1263.
[12] Z.-Q. Gao, A. Agarwal, A.D. Trigg, N. Singh, C. Fang, C.-H. Tung, Y. Fan, K.D. Buddharaju, J.-M. Kong, Anal. Chem. 79 (2007) 3291–3297.
[13] Y.L. Bunimovich, Y.S. Shin, W.-S. Yeo, M. Amori, G. Kwong, J.R. Heath, J. Am. Chem. Soc. 128 (2006) 16323–16331.
[14] G.-J. Zhang, G. Zhang, J.H. Chua, R.E. Chee, E.H. Wong, A. Agarwal, K.D. Buddharaju, N. Singh, Z.Q. Gao, N. Balasubramanian, Nano Lett. 8 (2008) 1066–1070.
[15] A. Cattani-Scholz, D. Pedone, M. Dubey, S. Neppl, B. Nickel, P. Feulner, J. Schwartz, G. Abstreiter, M. Tornow, ACS Nano. 2 (2008) 1653–1660.
[16] G.-J. Zhang, J.H. Chua, R.E. Chee, A. Agarwal, S.M. Wong, K.D. Buddharaju, N. Balasubramanian, Biosens. Bioelectron. 23 (2008) 1701–1707.
[17] G.-J. Zhang, J.H. Chua, R.E. Chee, A. Agarwal, S.M. Wong, Biosens. Bioelectron. 24 (2009) 2504–2508.
[18] G.-J. Zhang, Z.H.H. Luo, M.J. Huang, G.K. Tay, E.-J. Lim, Biosens. Bioelectron. 25 (2010) 2447–2453.
[19] G.-J. Zhang, L. Zhang, M.J. Huang, Z.H.H. Luo, G.K. Tay, E.-J. Lim, T.G. Kang, Y. Chen, Sens. Actuator B: Chem. 146 (2010) 138–144.
[20] A. Gao, N. Lu, P. Dai, T. Li, H. Pei, X. Gao, Y. Gong, Y. Wang, C. Fan, Nano Lett. 11 (2011) 3974–3978.
[21] G. Zheng, F. Patolsky, Y. Cui, W.U. Wang, C.M. Lieber, Nat. Biotechnol. 23 (2005) 1294–1301.
[22] E. Stern, J.F. Klemic, D.A. Routenberg, P.N. Wyremebak, D.B. Turner-Evans, A.D. Hamilton, D.A. LaVan, T.M. Fahmy, M.A. Reed, Nature 445 (2007) 519–522.
[23] A. Kim, C.S. Ah, H.Y. Yu, J.H. Yang, I.B. Baek, C.G. Ahn, C.W. Park, M.S. Jun, S. Lee, Appl. Phys. Lett. 91 (2007) 103901.
[24] J. Chua, R.E. Chee, A. Agarwal, S.M. Wong, G.-J. Zhang, Anal. Chem. 81 (2009) 6266–6271.
[25] H.S. Lee, K.S. Kim, C.J. Kim, S.K. Hahn, M.H. Jo, Biosens. Bioelectron. 24 (2009) 1801–1805.
[26] N.N. Mishra, W.C. Maki, E. Cameron, R. Nelson, P. Winterrowd, S.K. Rastogi, B. Filanoski, G.K. Maki, Lab Chip 8 (2008) 868–871.
[27] R. Tian, S. Regonda, J. Gao, Y. Liu, W. Hu, Lab Chip 11 (2011) 1952–1961.
[28] S.-P. Lin, C.-Y. Pan, K.-C. Tseng, M.-C. Lin, C.-D. Chen, C.-C. Tsai, S.-H. Yu, Y.-C. Sun, T.-W. Lin, Y.-T. Chen, Nano Today 4 (2009) 235–243.
[29] T.W. Lin, P.J. Hsieh, C.L. Lin, Y.Y. Fang, J.X. Yang, C.C. Tsai, P.L. Chiang, C.Y. Pan, Y.T. Chen, Proc. Natl. Acad. Sci. U. S. A. 107 (2010) 1047–1052.
[30] G.-J. Zhang, Z.H.H. Luo, M.J. Huang, J.A.J. Ang, T.G. Kang, H.M. Ji, Biosens. Bioelectron. 28 (2011) 459–463.
[31] G.-J. Zhang, M. Huang, Z.H.H. Luo, G.K. Tay, E.-J. Lim, E.T. Liu, J.S. Thomsen, Biosens. Bioelectron. 26 (2010) 365–370.
[32] G.-J. Zhang, M. Huang, J. Ang, E.T. Liu, K.V. Desai, Biosens. Bioelectron. 26 (2011) 3233–3239.
[33] W.U. Wang, C. Chen, K.-h. Lin, Y. Fang, C.M. Lieber, Proc. Natl. Acad. Sci. U. S. A. 102 (2005) 3208–3212.
[34] F. Patolsky, B.P. Timko, G. Yu, Y. Fang, A.B. Greytak, G. Zheng, C.M. Lieber, Science 313 (2006) 1100–1104.
[35] B. Tian, T. Cohen-Karni, Q. Qing, X. Duan, P. Xie, C.M. Lieber, Science 329 (2010) 831–834.
[36] I. Park, Z. Li, X. Li, A.P. Pisano, R.S. William, Biosens. Bioelectron. 22 (2007) 2065–2070.
[37] F. Patolsky, G. Zheng, O. Hayden, M. Lakadamyali, X. Zhuang, C.M. Lieber, Proc. Natl. Acad. Sci. U. S. A. 101 (2004) 14017–14022.
[38] P. Nair, M. Alam, IEEE Trans. Electron Dev. 54 (2007) 3400–3408.
[39] W. Lu, C.M. Lieber, J. Phys. D: Appl. Phys. 39 (2006) R387–R406.
[40] D.H. Tong, S. Chen, W.G. van der Wiel, E.T. Carlen, A. van den Berg, Nano Lett. 9 (2009) 1015–1022.
[41] N. Elfstrom, R. Juhasz, I. Sychugov, T. Engfeldt, A.E. Karlstrom, J. Linnros, Nano Lett. 7 (2007) 2608.
[42] X.T. Vu, J.F. Eschermann, R. Stockmann, R. GhoshMoulick, A. Offenhausser, S. Ingebrandt, Phys. Status Solidi A 206 (2009) 426–434.
[43] T. Kudo, T. Kasama, T. Ikeda, Y. Hata, S. Tokonami, S. Yokoyama, T. Kikkawa, H. Sunami, T. Ishikawa, M. Suzuki, K. Okuyama, T. Tabei, K. Ohkura, Y. Kayaba, Y. Tanushi, Y. Amemiya, Y. Cho, T. Monzen, Y. Murakami, A. Kuroda, A. Nakajima, Jpn. J. Appl. Phys. 48 (2009) 06FJ04.
[44] G. Pennelli, Microelectron. Eng. 86 (2009) 2139.
[45] O. Knopfmacher, A. Tarasov, W.Y. Fu, M. Wipf, B. Niesen, M. Calame, C. Schonenberger, Nano Lett. 10 (2010) 2268–2274.
[46] Y.B. Zhang, Y. Xiong, X.A. Yang, Y. Wang, W.H. Han, F.H. Yang, J. Nanosci. Nanotechnol. 10 (2010) 7113–7116.
[47] J.B. Reddy, O.H. Elibol, P.R. Nair, B.R. Dorvel, F. Butler, Z. Ahsan, D.E. Bergstrom, M.A. Alam, R. Bashir, Anal. Chem. 83 (2011) 888–895.
[48] J.B. Reddy Jr., R. Brian, J. Dorvel, P. Go, O.H. Nair, G.M. Elibol, J.S. Credo, E.K.C. Daniels, M. Chow, M.A. Madoo, R. Alam, Bashir, Biomed. Microdev. 13 (2011) 335–344.
[49] C.X. Xiang, S.C. Kung, D.K. Taggart, F. Yang, M.A. Thompson, A.G. Güell, Y. Yang, R.M. Penner, ACS Nano 2 (2008) 1939–1949.
[50] D. Engstrom, V. Savu, X. Zhu, I.Y.Y. Bu, W. Milne, J. Brugger, P. Boggild, Nano Lett. 11 (2011) 1568–1574.
[51] X.T. Vu, R. GhoshMoulick, J.F. Eschermann, R. Stockmann, A. Offenhusser, S. Ingebrandt, Sens. Actuator B: Chem. 144 (2010) 354–360.
[52] A. Agarwal, K. Buddharaju, I.K. Lao, N. Singh, N. Balasubramanian, D.L. Kwong, Sens. Actuators A: Phys. 145 (1) (2008) 207–213.
[53] I. Park, Z. Li, A.P. Pisano, R.S. William, Nano Lett. 7 (2007) 3106–3111.
[54] J. Israelachvili, Intermolecular and Surface Forces, Academic Press Inc., 1985.
[55] E. Stern, R. Wagner, F.J. Sigworth, R. Breaker, T.M. Fahmy, M.A. Reed, Nano Lett. 7 (2007) 3405–3409.
[56] C.W. Wang, C.Y. Pan, H.C. Wu, P.Y. Shih, C.C. Tsai, K.T. Liao, L.L. Lu, W.H. Hsieh, C.D. Chen, Y.T. Chen, Small 3 (2007) 1350–1355.
[57] P.R. Srinivas, B.S. Kramer, S. Srivastava, Lancet Oncol. 2 (2001) 698–704.
[58] D. Sidransky, Nat. Rev. Cancer 2 (2002) 210–219.
[59] R. Etzioni, N. Urban, S. Ramsey, M. McIntosh, S. Schwartz, B. Reid, J. Radich, G. Anderson, L. Hartwell, Nat. Rev. Cancer. 3 (2003) 243–252.

[60] E. Stern, A. Vacic, N.K. Rajan, J.M. Criscione, J. Park, B.R. Ilic, D.J. Mooney, M.A. Reed, T.M. Fahmy, Nat. Nanotechnol. 5 (2010) 138–142.
[61] G.A. Calin, G.G. Liu, C. Sevignani, M. Ferracin, N. Felli, C.D. Dumitru, M. Shimizu, A. Cimmino, S. Zupo, M. Dono, M.L. Dell'Aquila, H. Alder, L. Rassenti, T.J. Kipps, F. Bullrich, M. Negrini, C.M. Croce, Proc. Natl. Acad. Sci. U. S. A. 101 (2004) 11755–11760.
[62] M. Lagos-Quintana, R. Rauhut, W. Lendeckel, T. Tuschl, Science 294 (2001) 853–858.
[63] G.A. Calin, C.M. Croce, Cancer Res. 66 (2006) 7390–7394.
[64] P.T. Nelson, D.A. Baldwin, L.M. Scearce, J.C. Oberholtzer, J.W. Tobias, Z. Mourelatos, Nat. Methods 1 (2004) 155–161.
[65] R.M. Evans, Science 240 (1988) 889–895.
[66] D. Moras, H. Gronemeyer, Curr. Opin. Cell Biol. 10 (1998) 384–391.
[67] X.D. Su, C.Y. Lin, S.J. O'Shea, H.F. Teh, W.Y.X. Peh, J.S. Thomsen, Anal. Chem. 78 (2006) 5552–5558.
[68] D. Yach, S.R. Leeder, J. Bell, B. Kistnasamy, Science 307 (2005) 317.
[69] M. Muller-Bardorff, K. Hallermayer, A. Schroder, C. Ebert, A. Borgya, W. Gerhardt, A. Remppis, J. Zehelein, H.A. Katus, Clin. Chem. 43 (1997) 458–466.
[70] E.S. McErlean, S.A. Deluca, F. van Lente, F. Peacock 4th, J.S. Rao, C.A. Balog, S.E. Nissen, Am. J. Cardiol. 85 (2000) 421–426.
[71] M.S. Sabatine, D.A. Morrow, J.A. de Lemos, C.M. Gibson, S.A. Murphy, N. Rifai, C. McCabe, E.M. Antman, C.P. Cannon, E. Braunwald, Circulation 105 (2002) 1760–1763.
[72] G.-J. Zhang, K.T.C. Chai, Z.H. Luo, M. Huang, G.K. Tay, E.-J. Lim, M. Je, Biosens. Bioelectron. 35 (2012) 218–223.
[73] F.R.R. Teles, D.M.F. Prazeres, J.L. Limo-Filho, Rev. Med. Virol. 15 (2005) 287–302.
[74] A. Balmaseda, M. Guzman, S. Hammond, G. Robleto, C. Flores, Y. Tellez, E. Videa, S. Saborio, L. Perez, E. Sandoval, Y. Rodriguez, E. Harris, Clin. Diag. Lab. Immunol. 10 (2003) 317–322.
[75] N. Sadon, A. Delers, R.G. Jarman, C. Klungthong, A. Nisalak, R.V. Gibbons, V. Vassilev, J. Virol. Methods 153 (2008) 1–6.
[76] D.W. Vaughn, S. Green, S. Kalayanarooj, B.L. Innis, S. Nimmannitya, S. Suntayakorn, T.P. Endy, B. Raengsakulrach, A.L. Rothman, F.A. Ennis, A. Nisalak, J. Infect. Dis. 181 (2000) 2–9.
[77] F.S. Dawood, S. Jain, L. Finelli, M.W. Shaw, S. Lindstrom, R.J. Garten, L.V. Gubareva, X. Xu, C.B. Bridges, T.M. Uyeki, N. Engl. J. Med. 360 (2009) 2605–2615.
[78] A.C. Hurt, C. Baas, Y.M. Deng, S. Roberts, A. Kelso, I.G. Barr, Influenza Other Respir Viruses 3 (2009) 171–176.
[79] L.T.-H. Kao, L. Shankar, T.G. Kang, G.-J. Zhang, G.K. Tay, S.R.M. Rafei, C.W.H. Lee, Biosens. Bioelectron. 26 (2011) 2006–2011.